Plasma Medicine, 12(3):23–40 (2022)

Impact of Direct Plasma Jet and Indirect Plasma Activated Mist on Surface Properties of Different Material Samples during Bacterial Inactivation

Mohamed El Shaer,[a,*] Hossam Fayed,[a] Hanaa I. Abd El-Hady,[b] Ashraf El Sebaei,[a] & Mona Mobasher[a]

[a]Plasma & Energy Applications Research Laboratory, Department of Engineering Physics and Mathematics, Faculty of Engineering, Zagazig University, Zagazig, Egypt; [b]Department of Medical Microbiology and Immunology, Faculty of Medicine, Zagazig University, Zagazig, Egypt

*Address all correspondence to: Mohamed El Shaer, Faculty of Engineering, Zagazig University, Zagazig, 44599, Egypt; Tel.: +20-100-695-0077; Fax: +20552304987, E-mail: melshaer2901@gmail.com

ABSTRACT: During plasma surface decontamination of hospitals' accommodations and medical instruments, one should expect some changes to occur on the surfaces of different materials exposed to plasma. In this study we have investigated effects of cold atmospheric plasma on four common materials likely to be found in medical facilities, namely medical polyvinyl chloride, polystyrene, stainless steel, and borosilicate glass. Two plasma configurations are used, one directly using an atmospheric pressure plasma jet (APPJ) and the other indirectly using plasma activated mist through a gliding arc discharge producing plasma activated mist. After plasma treatment, surface properties of the considered materials are investigated using water drop analysis, attenuated total reflectance Fourier transform infrared spectroscopy, and atomic force microscopy. Plasma is found to reduce bacterial contamination and on the same time alters, in different proportions, surface materials' properties such as wettability, surface energy, and roughness, of the treated samples. We have found that although direct plasma using APPJ can act more rapidly than indirect plasma concerning bacterial elimination from different materials' surfaces, indirect application through plasma activated mist is able to achieve the same bacterial death rate on longer time periods. This can be advantageous due to mild and best penetrating behavior of plasma activated mist on sensitive medical installations.

KEY WORDS: cold atmospheric plasma, gliding arc discharge, PVC, stainless-steel, wettability, roughness, plasma activated mist, *E. coli*

I. INTRODUCTION

Cold atmospheric plasma (CAP) has shown interesting properties in many fields such as medicine, agriculture, food, and wastewater treatment.[1] Owing to the local production of a combination of reactive oxygen species (ROS), reactive nitrogen species (RNS) and UV light. CAP has been very effective in many fields particularly in decontamination and disinfection by elimination of microorganisms from different surfaces.[2] However, as CAP acts differently on various materials' surfaces, this should be carefully examined during plasma application.[3]

1947-5764/22/$35.00

In this work, we will consider the effects of plasma during bacterial decontamination on materials normally found in hospitals, households, and workplaces. We will explore four materials: medical polyvinyl chloride (PVC), polystyrene (PS), medical stainless steel (SS), and borosilicate glass (BSG). The effects of CAP on those materials have been extensively studied by many authors. First, considering PVC, which is a high strength thermoplastic material widely used in many medical devices as nebulizer masks, blood storage bags, and catheters. Suganya et al.[4] studied the effect of air, argon, and oxygen DC glow discharge of plasma on PVC film. They have found that glass transition temperature slightly increased for oxygen plasma treated material due to the presence of higher concentration of polar functional groups. Gui and Wang[5] treated PVC with plasma to study changes of wettability and surface cohesiveness. They have found that the contact angles of PVC treated by plasma have been changed leading to an obvious improvement in surface wettability, and that shear strength had shown a significant increase in surface bonding performance. Second, considering PS, which is a hard solid plastic often used in products that require clarity, such as food packaging and laboratory ware like cell culture plates. Fricke et al.[6] used different surface preparation techniques to equip surfaces with functional groups to improve initial surface interactions. PS surfaces were modified by using different nonthermal plasma processes. Low-pressure plasma and atmospheric-pressure plasma have been applied to modify surfaces or to deposit thin films on surfaces. They have found that the functionalization of PS substrates by applying low-pressure and atmospheric-pressure plasma processes were equally effective in the improvement of cell attachment and proliferation. Vida et al.[7] used diffuse coplanar surface barrier discharge producing atmospheric pressure ambient air plasma for treatment of PS foils. They have found that short plasma treatment time leads to an improved wetting of the surface, while longer treatment times having little or no effect on further improvement of the hydrophilicity of the surface. Also, better wettability was correlated with decreasing carbon to oxygen ratio resulting from an incorporation of oxygen-containing functional groups C–OH, C=O, and O–C=O during surface oxidation. Third, considering medical grade stainless steel (SS), which is an austenitic stainless steel known for its high formability and exceptional corrosion resistance. Grade 316 stainless steels contain high levels of nickel which provide additional chemical properties, making it suitable for use within the extreme demands of the medical industry as for biomedical implants and surgical or dental instruments.

Kim et al.[8] used the atmospheric pressure plasma jet method at room temperature to modify the stainless-steel surface, which have been characterized by contact angle analyzer. They have found that the surface energy of treated SS was increased remarkably when compared to the untreated one and that the main functional groups, causing the change in hydrophilic surface were generated under the surface reactions caused by reactive etching and oxidation of ions and activated species in the plasma. Williams et al.[9] used CAP to modify 316 SS surfaces and they have found that after a short exposure time to the plasma torch, surface free energy increased as compared to as-received

surfaces. They suggested that the mechanism that causes the increase in surface free energy is chain scission of the hydrocarbon contamination triggered by free electrons in the plasma plume followed by chemical functionalization of the metal oxide surface and some of the remaining carbon contamination layer.

Fourth, considering BSG, which is commonly used in medical and pharmaceutical applications owing to its very low coefficient of thermal expansion making it less subjected to thermal stress, and its physical durability resulting from high material strength. Lim and Lee[10] studied glass and glass fibers exposed to dry interfacial treatment using plasma technology. They have found that the optimum parameters for best wettability of the samples at the time of plasma generation occurred in an oxygen atmosphere. Homola et al.[11] studied the treatment of flat glass surfaces by ambient air atmospheric pressure plasma, generated by a diffuse coplanar surface barrier discharge. They have found that an enhancing influence of the glass surface itself on diffuse plasma was observed and explained by different discharge onsets and changes in the electric field distribution.

Considering bacterial surface decontamination by CAP, plasma can be applied either directly on materials surfaces by atmospheric pressure plasma jet (APPJ) and dielectric barrier discharge (DBD) or indirectly through a plasma activated medium (PAM) which can be plasma activated water (PAW) or plasma activated mist (PAMi). Fridman et al.[12] investigated the effectiveness of non-thermal atmospheric pressure floating electrode dielectric barrier discharge plasma in interaction with living organisms. Two regimes were analyzed: one where this plasma comes in direct contact with the organism and the other where plasma is separated from the treatment target by a grounded mesh. They have found that direct plasma contact is more efficient for sterilization due to charged species delivered by plasma to the surface of the organism.

Sysolyatina et al.[13] used plasma-activated water mist obtained by the ignition of plasma within an air-vapor mixture which have showed significant antibacterial properties by decreasing loads of foodborne pathogens by large factors in very short time as *Listeria monocytogenes*, *Escherichia coli*, and *Salmonella enterica* serovar Typhimurium. Their results suggested the importance of short-lived radicals' antibacterial treatment. Yahaya et al.[14] investigated direct and indirect bactericidal effects of dielectric barrier discharge microplasma in air and plasma jet generated in an argon-oxygen gas mixture producing plasma activated water. They have found that the indirect method using plasma activated water may increase the bacterial inactivation area since a liquid medium could be spread on large surfaces. Kim and Kim[15] found that in the medical field, plasma-activated liquid would have large capabilities of accessing places where direct applications of plasma may be difficult. In the following investigations, we will examine materials properties as wettability, surface energy and roughness as related to the decontamination efficacy of plasma using direct plasma jet and indirect plasma activated mist in air for different materials seeded by *E. coli* as one of most common causes of healthcare-associated infections.[16]

II. MATERIALS AND METHODS

A. Sample Preparation

We use specimens of four different materials. The first was medical grade PVC coupons of cubic shape of 2.0 × 2.0 cm^2 surface area and 0.2 cm thickness. The density of PVC is (ρ_{PVC} = 1.24 g/cm^3) and its molecular weight (M_{PVC} = 21.150 g/mol). Origin: mask for commercial ultrasonic nebulizer (model F-202.00, Fazzini Srl, Vimodrone (MI) Italy), sterile mask has been cut in pieces and flattened under moderate pressure for 30 minutes. The second material was PS specimens of 2.0 × 2.0 cm^2 and 0.1 cm thickness. The density of PS is (ρ_{PS} = 0.96 g/cm^3) and its molecular weight (M_{PS} = 104.1 g/mol). Origin: from 6-well cell culture plate, clear polystyrene not treated from Corning Coaster (USA). The third material was medical grade SS AISI 316 coupons of cubic shape of 2.0 × 2.0 cm^2 surface area and 0.2 cm thickness, SS density is (ρ_{SS} = 7.9 g/cm^3) and its molecular weight (M_{SS} = 20.376 g/mol). The SS flat coupons were obtained from a local supplier. The fourth and final material was BSG cover slips of cubic shape of 2.0 × 2.0 cm^2 and 0.017 cm thickness. The density of BSG is (ρ_{BSG} = 2.23 g/cm^3) and its molecular weight (M_{BSG} = 179.93 g/mol). Origin: glass slides from Ilmenau Glaswerke GMBH (Germany) 76 × 26 mm.

B. Direct Atmospheric Pressure Plasma Jet

Figure 1 shows the setup of the direct atmospheric plasma jet (APPJ). The cathode is a tungsten rod of 150 mm long and 3.2 mm diameter covered by a ceramic insulator and the anode is a copper cylinder of 30 mm height and 54 mm outer diameter containing on its middle an exit nozzle of 3.2 mm diameter. The discharge occurs inside the torch in the gap between the cathode tip and the exist nozzle. The plasma extends outward due to the injection of compressed air with volume flow rate of 12 SLM introduced through a helical path of 8 mm pitch to create a stabilizing swirl air motion.[17] The sample surfaces were exposed to plasma jet at 3.5 cm from the nozzle. The electric power supply is a half wave rectified signal made by a 220 V- 4 kV step-up transformer, delivering 400 VA followed by a high voltage diode HVM12, a 1.05 μF capacitor and 5 kΩ Resistor. The voltage and current characteristics are shown in Fig. 2.

Gliding arc discharge (GAD) has been used for surface treatment of different polymers, to induce surface modifications.[18] Figure 3 shows the setup arrangement and details of knife shape electrodes.

The mist generator is made by a commercial mist maker with 10 ultrasonic transducers submerged in a tank with a constant water level. The ultrasonic transducer is composed by a piezoelectric crystal and a ceramic disc with a diameter of 16 mm. The transducer can convert high frequency electrical signals, which generally range from 0.8 to 1.65 MHz, into high frequency mechanical vibrations on the disc when submerged in water, producing thin water mist with droplet sizes of a few tens of microns. Water mist is introduced in the space between the two electrodes through a Teflon tube assuring

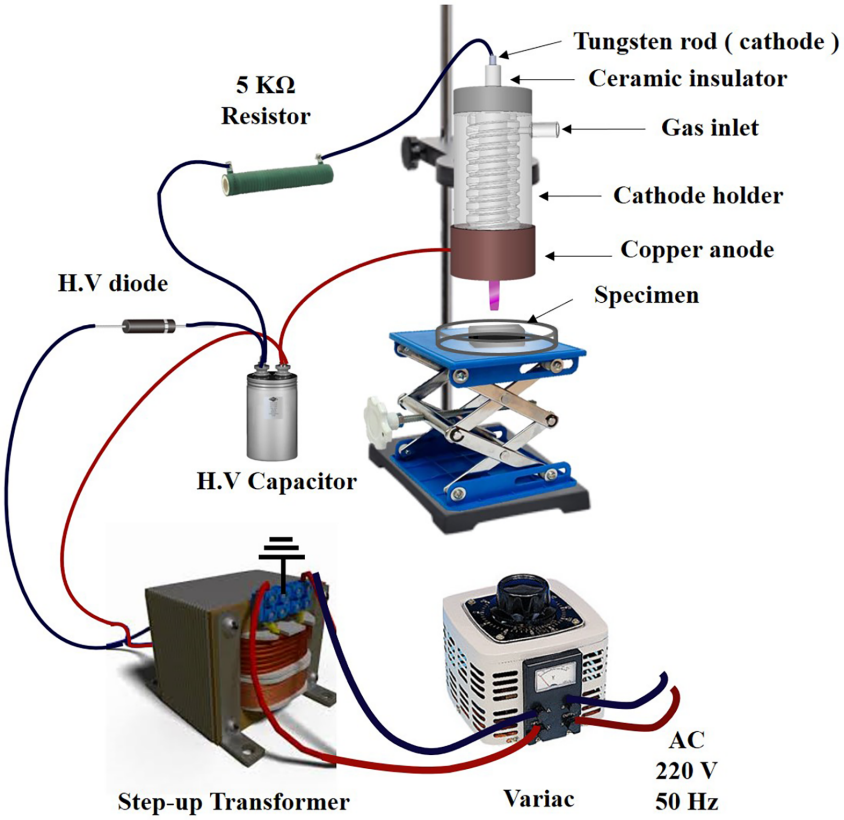

FIG. 1: Setup of the APPJ

good mixing between mist and inlet compressed air used as working gas. This GAD consists of two knife-shaped stainless-steel electrodes of 80 mm long, 20 mm wide on its largest position, and 4 mm thick. AC power source is supplied by a neon-sign transformer giving up to 9 kV and 30 mA. The secondary of the transformer is center-tapped and the two outputs are connected to the two opposite knife shaped electrodes of the GAD, as indicated in Fig. 3, to initiate the necessary voltage for arc ignition. The working gas is air, produced by a compressor, with a volume flow rate of 12 SLM applied through a Teflon tube terminated by a 2 mm nozzle positioned between the two electrodes as shown in Fig. 3. The spacing between the electrodes' lower extreme tips and the specimen is fixed at 5 cm, and the gap at the electrodes' neck is adjusted to around 2 mm. The applied voltage and current characteristics are shown in Fig. 4.

C. Infrared Thermal Analysis

Infrared images of specimens have been obtained during plasma treatment using a thermal imager sensor FLIR A5sc (Oregon, USA) with spatial resolution of 2.78 mrad and

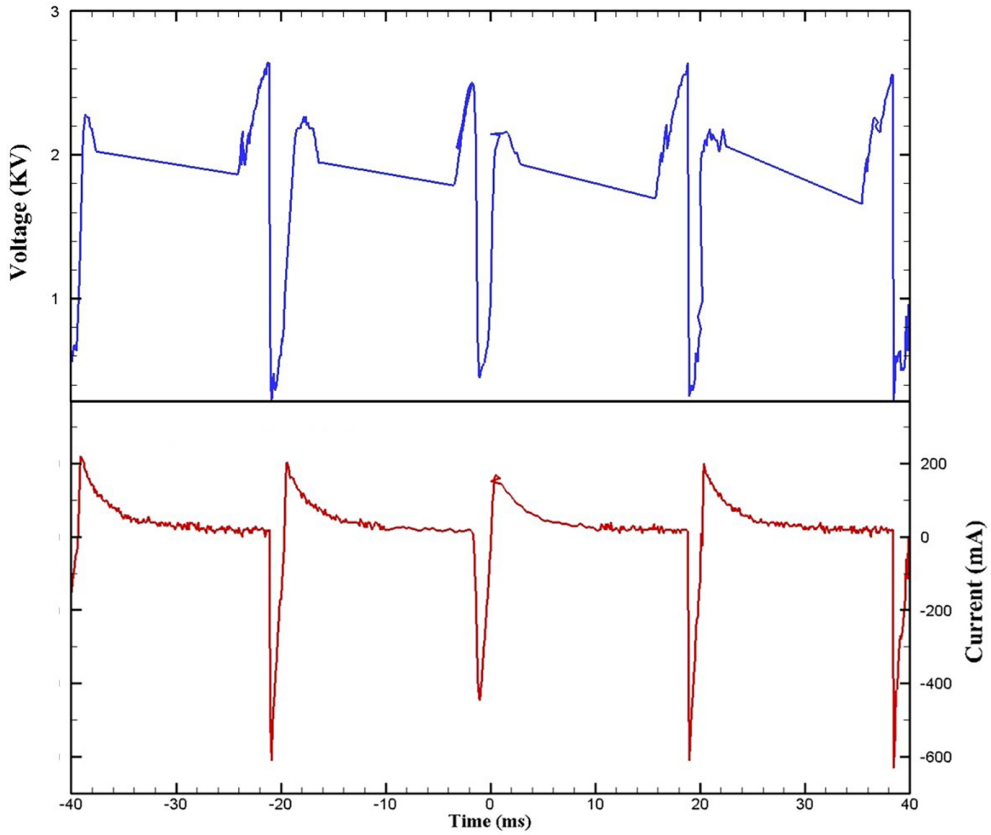

FIG. 2: Voltage and current characteristics as applied to APPJ

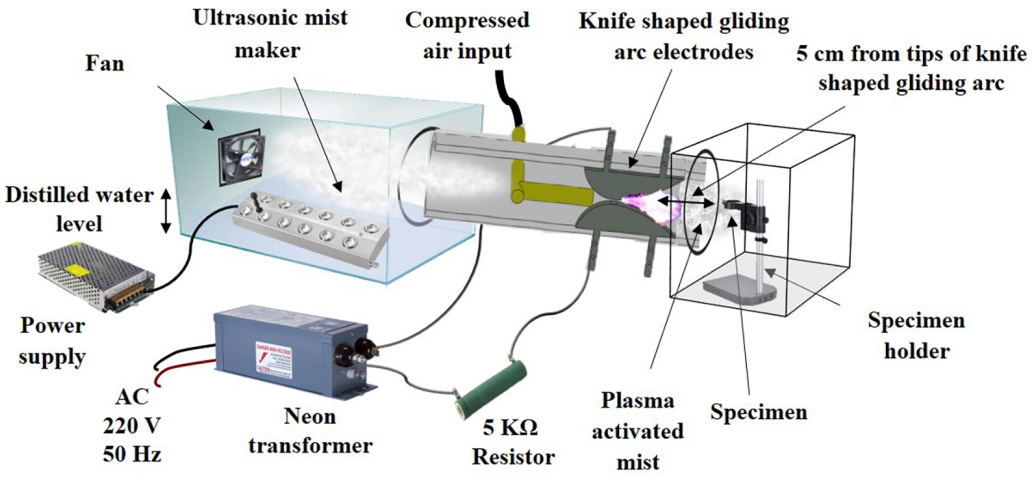

FIG. 3: Setup of GAD with details of electrodes

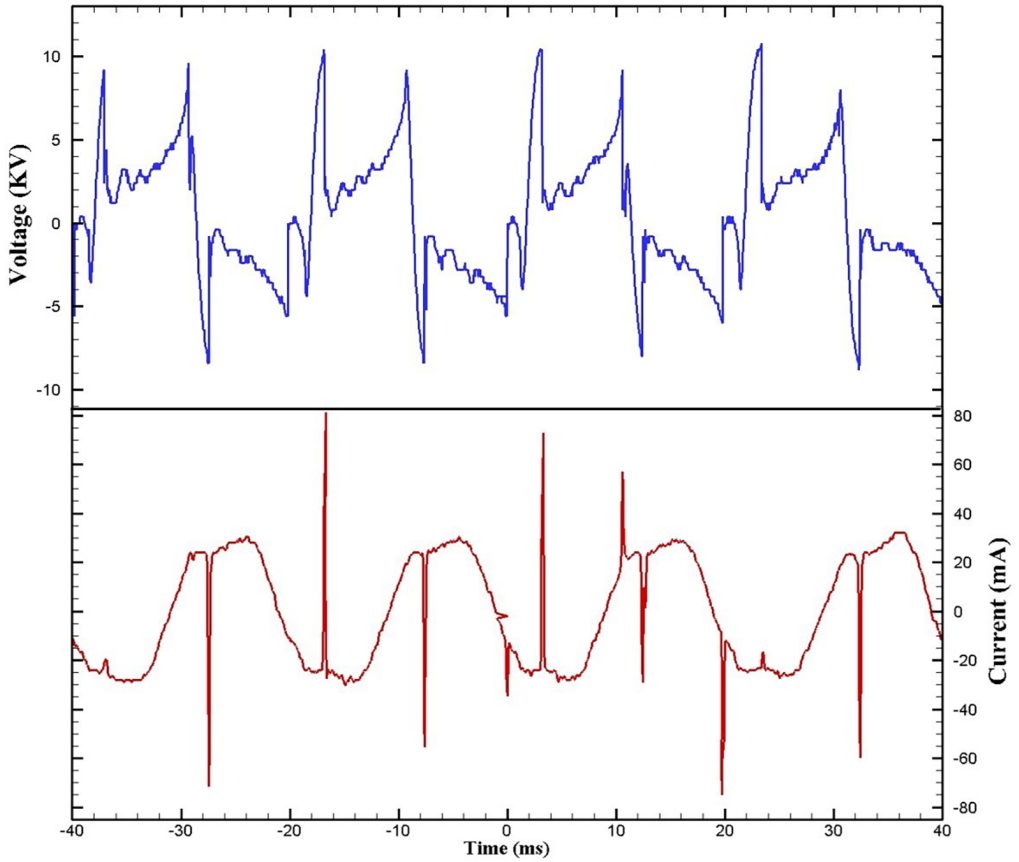

FIG. 4: Voltage and current characteristics as applied to GAD

spectral resolution of 7.5–13 μm. The infrared (IR) sensor is set 20 cm from specimen with an inclination angle of 45°. The sensor is focused on an area of 0.38 cm^2 on the middle of the treated specimen of 2.0 × 2.0 cm^2. Measuring conditions were as follows: ambient temperature 25°C, relative humidity 60%. The IR emissivity e for PVC is taken to be 0.91. For APPJ, plasma voltage of 2650 V and arc current of 50 mA was used. Specimen surface average temperature was measured at different exposure time starting from ambient temperature of 25°C. Figure 5 shows the IR image of the APPJ directed on PVC specimen which is the most vulnerable material to heat load by plasma.

In stationary conditions directly after shutting down the plasma. We observe the temperature distribution on a circular area corresponding to the jet diameter of about 3 mm (diameter of the nozzle). After 120 s of plasma treatment the temperature is around 40°C and decrease outward the center of the specimen. On a spot at the center of the treated area, the temperature is observed to decrease slightly due to the cooling action of the injected air used to sustain the plasma. Plasma region shows no infrared emission which indicated the nonthermal nature of the plasma. For GAD the temperature of the

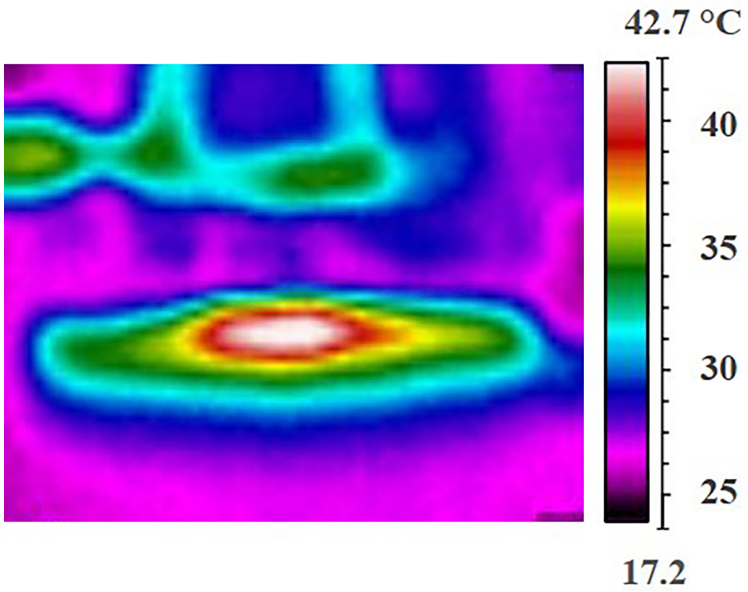

FIG. 5: IR camera surface temperature after 120 s of treatment with APPJ

specimen treated by PAMi is measured to be around room temperature, no temperature increase is observed 5 cm from the electrodes.

D. Wettability, Contact Angle, and Surface Free Energy of Specimen Surface

Wettability of a liquid on a solid surface, is characterized by the water contact angle (WCA) θ which is the angle between the solid surface and the tangent to the surface of the liquid drop at that point. WCA can be determined by the *sessile* drop technique,[19] in which a droplet of liquid is deposited by a syringe which is positioned above the sample surface, and a digital camera captures the image which is then analyzed by eye. The contact angle θ is given by Young's equation:[20]

$$\cos\theta = \frac{\gamma_{sv} - \gamma_{sl}}{\gamma_{lv}} \quad (1)$$

where γ_{sv} is the surface free energy of solid substrate against vapor or the surface tension of solid, γ_{lv} is the surface free energy of liquid against vapor or the surface tension of liquid, and γ_{sl} is the solid-liquid interfacial free energy. Equation (1) shows that wetting is favored by a high solid surface tension, a low solid-liquid interfacial free energy, and a low liquid surface tension.

The surface energy is calculated using the two liquid method distilled water and glycerol with known p (polar component) and d (dispersive component). The polar and dispersive components of the surface energy of the polymer film surface were calculated using the Fowke's approximation:[21]

$$\gamma_l(1+\cos\theta) = 2\left(\gamma_l^d\gamma_s^d\right)^{1/2} + 2\left(\gamma_l^p\gamma_s^p\right)^{1/2} \quad (2)$$

where θ is the testing liquids' contact angle, γ_l is the liquid surface tension, and γ_l^p and γ_l^d are the test liquids' polar and dispersive components. Similarly, γ_s the polar and dispersive components of solid-surface tension (s) are represented:

$$\gamma_s = \gamma_s^p + \gamma_s^d \quad (3)$$

For two liquids i and j:

$$\gamma_{li}(1+\cos\theta_i) = 2\left(\gamma_{li}^d\gamma_s^d\right)^{1/2} + 2\left(\gamma_{li}^p\gamma_s^p\right)^{1/2} \quad (4)$$

$$\gamma_{lj}(1+\cos\theta_j) = 2\left(\gamma_{lj}^d\gamma_s^d\right)^{1/2} + 2\left(\gamma_{lj}^p\gamma_s^p\right)^{1/2} \quad (5)$$

By using the values of the surface tension and the polar and dispersive components of the test liquids, the components of the surface energy of the solid γ_s^p and γ_s^d can be determined from Eqs. (4) and (5), and their sum will give the total energy of the solid. The two liquids water and glycerol with known γ^p (polar component) and γ^d (dispersive component) were used for calculating the surface energy of materials. The values of polar and dispersive components of testing liquids are given in Table 1. Three readings were taken at different places of the sample surface and an average have been determined. The polar and dispersive components of the surface energy of the polymer film surface are then calculated as described above.

TABLE 1: Surface energy of liquids used

Liquid	γ_l(mJ/m^2)	γ_l^d (mJ/m^2)	γ_l^p (mJ/m^2)
Distilled water	72.8	21.8	51.0
Glycerol	64.0	34.0	30.0

E. Specimen Surface Analysis

The surface topography of treated SS and PVC specimens was investigated using an atomic force microscope (AFM, FlexAFM Nanosurf AG, Switzerland). The samples have been scanned by contact mode. The image size was 10 μm with a constant force 20 nN in air environment with a temperature 20–25°C. Another technique have been used for infrared analysis on polymer samples by attenuated total reflectance-Fourier transform infrared (ATR-FTIR) spectroscopy which is a fast technique allowing the identification of chemical changes occurring on the polymer surface due to plasma treatment. The measurements have been performed using an FTIR spectrometer Vertex 70 (Bruker-Germany) equipped with vertical ATR device which is a surface sensitive method due to its inherent low depth of penetration. The spectrometer is continuously purged with nitrogen gas. The internal reflection element is a diamond crystal. Total 32 scans per analysis were used with a resolution of 4 cm^{-1} are taken for spectrum integration in the wavenumber range from 4000 to 400 cm^{-1}. ATR-FTIR analysis is carried out on the untreated and plasma treated specimens.

F. Measurements of Bacterial Inactivation on Plasma Treated Materials

A non-multidrug resistant bacterial strain used in this study was *E. coli*, Gram-negative bacteria microbiologically identified by conventional method (growth character, colonial morphology, gram-stained film, and biochemical reactions). For preparation of a master suspension using *E. coli* strain, density of bacteria was visually adjusted to 0.5 McFarland turbidity standard from bioMérieux SA, France. Using calibrated loop, 10 μl of this master suspension was subsequently spread on equal sized samples of PVC, PS, SS, and BSG, each of them sized 2 cm × 2 cm and dried for 30 min in the ambient air under the safety workbench. Immediately after the drying process, the seeded samples were placed in the treatment chamber, each material exposed to CAP for different treatment time periods from 15, to 120 s and to PAMi for longer treatment time periods from 15, to 600 s depending on the specimens' materials. After treatment, each sample was added to 10 ml of sterile media, vortexed for 1 min. Using calibrated loop 10 μl of the recovered suspension were placed on nutrient agar plate to evaluate the number of survived bacteria. The agar plates were then incubated for up to 24 hours at 37°C. After incubation, the number of colony-forming units (CFU) was counted to evaluate the log reduction compared to control.

III. RESULTS AND DISCUSSION

A. Wettability and Surface Energy of Material Surfaces by Plasma

Figure 6 shows the measured contact angles for the four material types considered treated by direct APPJ in air and indirect PAMi through GAD in air. From Fig. 6, we observe that contact angles decrease for the 4 materials in question with direct and

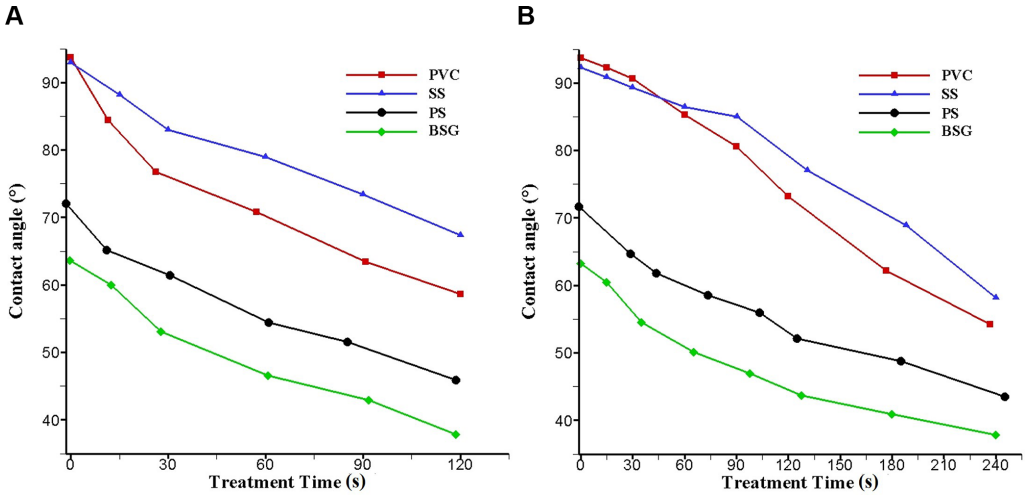

FIG. 6: Contact angles for four different materials using direct APPJ (A) and indirect PAMi (B).

indirect plasma exposures. This indicates that specimens' surfaces are becoming more hydrophilic. However, contact angles are decreasing with direct APPJ more rapidly than with indirect mist. For PAMi the treatment time is mostly doubled to observe noticeable values compared to those one's given during APPJ treatment. Figure 7 shows the surface energy calculated for the two cases.

We observe that surface energy of treated samples increases with increasing treatment time. Generally, a surface with a low surface energy will cause poor wetting and

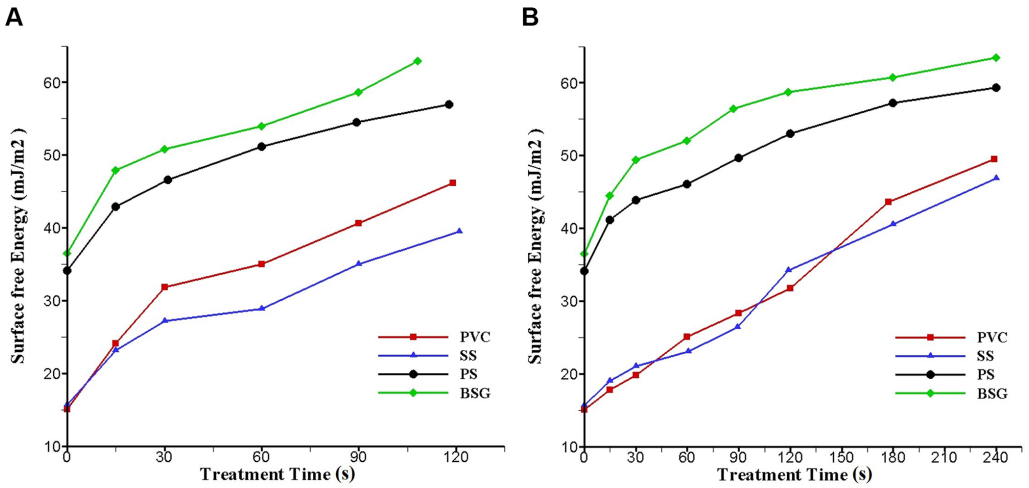

FIG 7: Surface energy of four different materials using APPJ (A) and PAMi (B)

therefore results in a high contact angle, which indicates that plasma by increasing the surface energy, ameliorate the wetting process.

B. Surface Morphology Changes due to Direct and Indirect Plasma Treatments

AFM has been used to investigate the morphology changes in the surface of PVC and SS specimens due to direct and indirect cold plasma treatments by measuring arithmetic mean height: S_A and root mean square height: S_q of the samples. Figure 8 shows the morphology of PVC samples in 3D and 2D representations for untreated

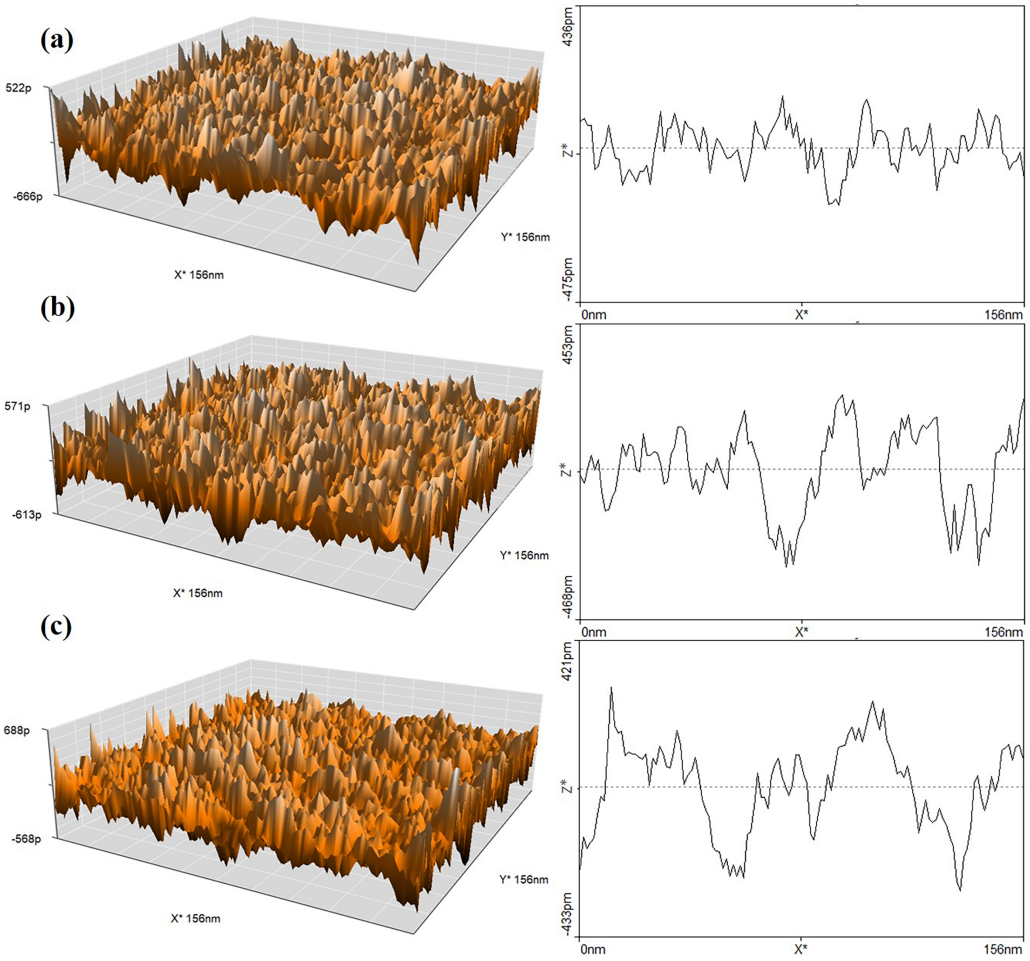

FIG. 8: Atomic force microscope for PVC specimens untreated (a), after 120 s of direct treatment by APPJ (b), and after 240 s of indirect treatment by PAMi (c). Left figures represent the 3D morphology and right figures correspond to the 2D representation (x–z).

sample and after an exposure time of 120 s to direct APPJ and 240 s to indirect PAMi. The measured values are listed in Table 2. Figure 9 shows the morphology of SS samples after an exposure time of 120 s to direct APPJ and 240 s to indirect

TABLE 2: Area roughness parameters for PVC

	Untreated	After 120 s of treatment with APPJ	After 240 s of treatment with PAMI
Arithmetic mean height: S_A	0.1103 nm	0.12189 nm	0.11976 nm
Root mean square height: S_q	0.13931 nm	0.15346 nm	0.15067 nm

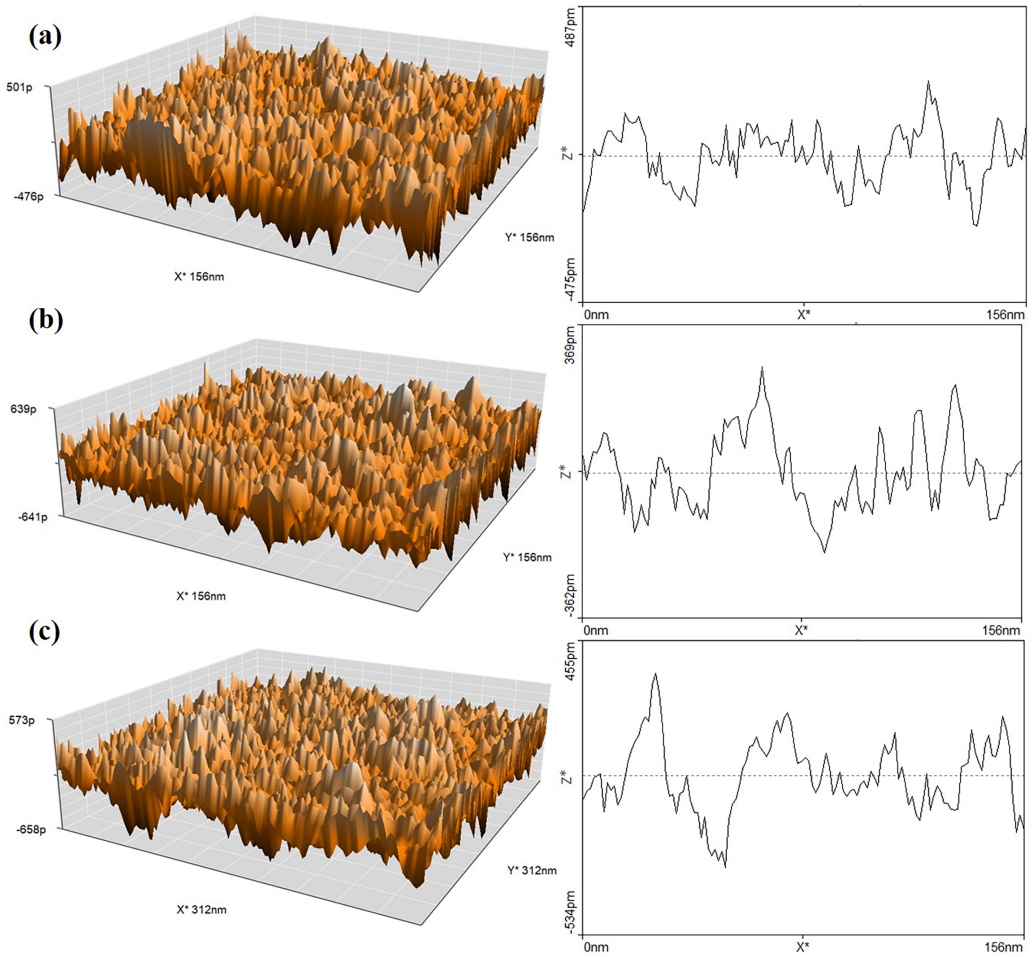

FIG. 9: Atomic force microscope for SS specimens untreated (a), after 120 s of direct treatment by APPJ (b), and after 240 s of indirect treatment with PAMi (c). Left figures represent the 3D morphology, and the right figures correspond to the 2D representation (x–z).

PAMi. samples in 3D and 2D representations for untreated sample and after an exposure time of 120 s to direct APPJ and 240 s to indirect PAMi. The measured values are listed in Table 3.

From values in Tables 2 and 3, we can remark only slight increases in area roughness parameters for PVC and SS treated specimens as compared to untreated ones. Values for 120 s direct treatment by APPJ and 240 s indirect treatment by PAMi are nearly comparable. Plasma in direct and indirect exposures produces reactive species which interacts with specimens' outer layers and may create etching effects leading to texture and tactile differences on the specimens' surfaces.[22] This change in roughness is not severe, which may be considered as a benefit during frequent use of plasma either directly or indirectly in disinfection limiting large changes in the treated materials.

C. FTIR Spectrum Analysis of PVC Polymer Surface

Figure 10 shows the ATR-FTIR spectra of PVC samples, for untreated, 120 s treated by APPJ and 240 s treated by PAMi. The peak in the spectrum at 1725 cm^{-1} representing the stretching vibration of C=O (carbonyl group) shows larger absorbance in (b) for sample treated by APPJ than untreated one in (a). This increase in absorbance is more moderate in (c) for samples treated by PAMi. The peak at 2470 cm^{-1} shows similar behavior for untreated and treated ones. The magnitudes of the large peak at 3520 cm^{-1} increases in the treated samples at b and c and can be assigned to stretching vibration of OH. Formation of such functional groups was found in air plasma discharges.[23] The increase of wettability and surface energy of plasma treated surfaces can be assigned to the incorporation of such new polar functional groups.

D. Antibacterial Activity of Plasma of Treated Materials

Figure 11 shows the effect of direct and indirect plasma on *E. coli* seeded on PVC specimens. The technique is repeated for PS, SS, and BSG. Effects of direct and indirect plasma on the four materials considered are shown in Fig. 12. We observe a decrease in bacteria cell viability by applying direct or indirect plasma to the specimens of different materials. However indirect wet exposure needs more time to kill bacteria with slower log reduction rate.

TABLE 3: Area roughness parameters for SS

	Untreated	**After 120 s of treatment with APPJ**	**After 240 s of treatment with PAMI**
Arithmetic mean height: S_A	0.10302 nm	0.12056 nm	0.11701 nm
Root mean square height: S_q	0.12934 nm	0.15229 nm	0.1479 nm

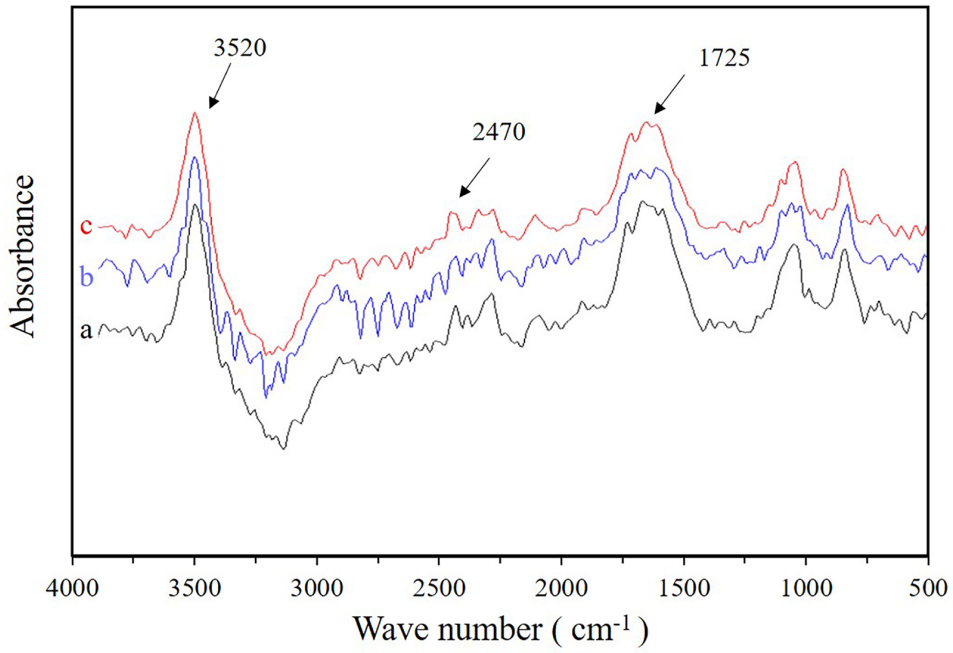

FIG. 10: ATR-FTIR spectrum for PVC samples untreated (a), after 120 s treatment with APPJ (b), and after 240 s of treatment with PAMI (c)

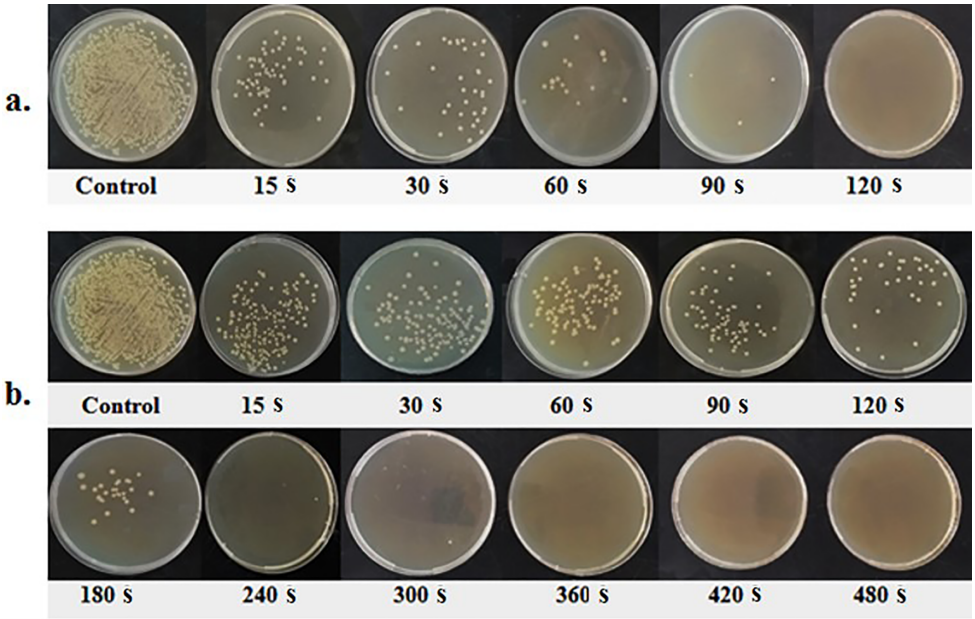

FIG. 11: *E. coli* on PVC treated with APPJ (a) or indirect PAMi (b)

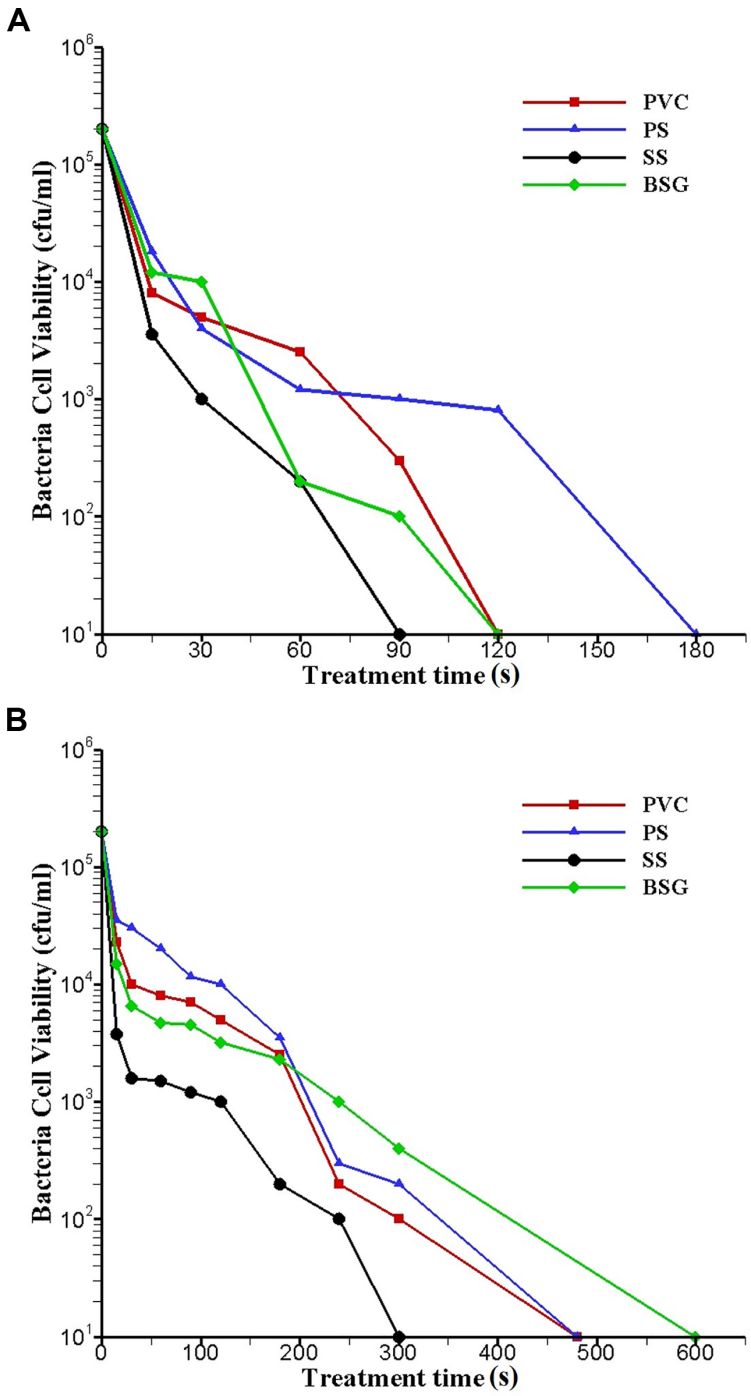

FIG. 12: *E. coli* (×10^5 cfu/ml) seeded on PVC, PS, SS, BSG for direct APPJ (A) or indirect PAMi (B)

IV. CONCLUSIONS

Comparisons between direct plasma application using APPJ and indirect plasma by PAMI through GAD show the effectiveness of the two methods in eliminating bacteria from solid samples. The plasma applications either directly or indirectly cause some changes in material surface morphology by increasing surface energy and corresponding wettability enhancement.

Specimens surface roughness for either direct or indirect plasma exposures slightly increase compared to the untreated cases, this may be related to surface etching by reactive species produced by plasma. Direct plasma using APPJ shows always rapid results than indirect plasma concerning changes occurring on the surface and bacterial elimination from different materials' surfaces. However, indirect application through plasma activated mist can achieve the same bacterial death rate on relatively longer time periods. This can be advantageous due to mild and best penetrating behavior of plasma activated mist on sensitive medical installations.

REFERENCES

1. Keidar M, Weltmann K-D, Macheret S. Fundamentals and applications of atmospheric pressure plasmas. J Appl Phys. 2021;130(8):080401.
2. Scholtz V, Pazlarova J, Souskova H, Khun J, Julak J. Nonthermal plasma – A tool for decontamination and disinfection. Biotechnol Adv. 2015;33(6 Part 2):1108–19.
3. Moritz S, Schmidt A, Sann J, Thoma MH. Surface modifications caused by cold atmospheric plasma sterilization treatment. J Phys D. 2020;53(32):325203.
4. Suganya A, Shanmugavelayutham G, Rodríguez CS. Study on structural, morphological and thermal properties of surface modified polyvinylchloride (PVC) film under air, argon and oxygen discharge plasma. Mater Res Exp. 2016;3(9):095302.
5. Gui R, Wang Z. Study on performance of polyvinyl chloride treated by plasma. IOP Conf. Ser.: Mater. Sci. Eng. 2019;472(1):012038.
6. Fricke K, Duske K, Quade A, Nebe B, Schroder K, Weltmann K-D, von Woedtke T. Comparison of nonthermal plasma processes on the surface properties of polystyrene and their impact on cell growth. IEEE Trans Plasma Sci. 2012;40(11):2970–9.
7. Vida J, Ilčíková M, Přibyl R, Homola T. Rapid atmospheric pressure ambient air plasma functionalization of Poly(styrene) and Poly(ethersulfone) foils. Plasma Chem Plasma Process. 2021;41(3): 841–54.
8. Kim MC, Song DK, Shin HS, Baeg SH, Kim GS, Boo JH, Han JG, Yang SH. Surface modification for hydrophilic property of stainless steel treated by atmospheric-pressure plasma jet. Surf Coat Technol. 2003;171(1-3):312–6.
9. Williams DF, Kellar EJC, Jesson DA, Watts JF. Surface analysis of 316 stainless steel treated with cold atmospheric plasma. Appl Surf Sci. 2017;403:240–7.
10. Lim K-B, Lee D-C. Surface modification of glass and glass fibres by plasma surface treatment. Surf Interface Anal. 2004;36(3):254–8.
11. Homola T, Matoušek J, Kormunda M, Wu LYL, Černák M. Plasma treatment of glass surfaces using diffuse coplanar surface barrier discharge in ambient air. Plasma Chem Plasma Process. 2013;33(5):881–94.
12. Fridman G, Fridman A, Gutsol A, Vasilets V, Friedman G. Comparison of direct and indirect effects of non-thermal atmospheric pressure plasma on bacteria and mechanisms of such interaction; 2007;

IEEE 34th International Conference on Plasma Science (ICOPS); 2007 June 17-22; Albuquerque, NM, USA: IEEE; 2007. p. 322.
13. Sysolyatina EV, Lavrikova AY, Loleyt RA, Vasilieva EV, Abdulkadieva MA, Ermolaeva SA, Sofronov AV. Bidirectional mass transfer-based generation of plasma-activated water mist with antibacterial properties. Plasma Process Polym. 2020;17(10):e2000058.
14. Yahaya AG, Okuyama T, Kristof J, Blajan MG, Shimizu K. Direct and indirect bactericidal effects of cold atmospheric-pressure microplasma and plasma jet. Molecules. 2021;26(9):2523.
15. Kim S, Kim CH. Applications of plasma-activated liquid in the medical field. Biomedicines. 2021;9(11):1700.
16. Fallon M, Kennedy S, Kumar S, Daniels S, Humphreys H. The potential use of a cold atmospheric plasma jet for decontamination of hospital surfaces. A pilot study. Plasma Med. 2021;11(1):15–30.
17. Patel AR, Shukla AN. Design and experiments on pen-shaped plasma torch for surface modification. Alex Eng J. 2018;57(4):3199–203.
18. Darvish F, Mostofi Sarkari N, Khani M, Eslami E, Shokri B, Mohseni M, Ebrahimi M, Alizadeh M, Dee CF. Direct plasma treatment approach based on non-thermal gliding arc for surface modification of biaxially-oriented polypropylene with post-exposure hydrophilicity improvement and minus aging effects. Appl Surf Sci. 2020;509:144815.
19. Bracco G, Holst B, Surface science techniques: Springer series in surface sciences. New York: Springer; 2013.
20. Makkonen L. Young's equation revisited. J Phys Condens Matter. 2016;28(13):135001.
21. Żenkiewicz M. Methods for the calculation of surface free energy of solids. J Achiev Mater Manuf Eng. 2007;24(1):137–45.
22. Mandolfino C, Lertora E, Gambaro C. Effect of cold plasma treatment on surface roughness and bonding strength of polymeric substrates. Key Eng Mater. 2014;611–612:1484–93.
23. Dave H, Ledwani L, Chandwani N, Kikani P, Desai B, Nema Sk. Surface modification of polyester fabric by non-thermal plasma treatment and its effect on coloration using natural dye. J Polym Mater. 2013;30(3):291–304.